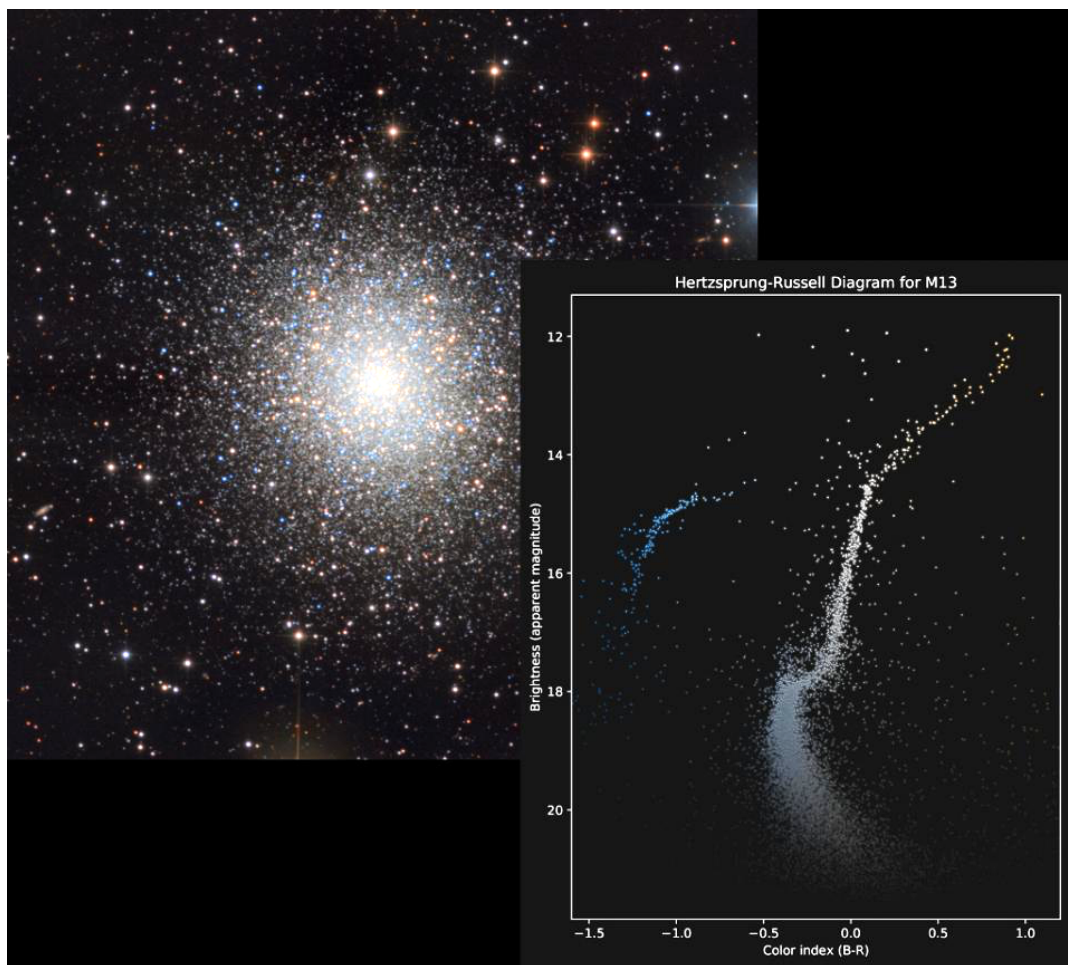


# Hertzsprung-Russell Diagrams For Clusters M13 and M6

*Globular and Open Clusters Comparison Study*



06.10.2023  
S23 PHYS 134L

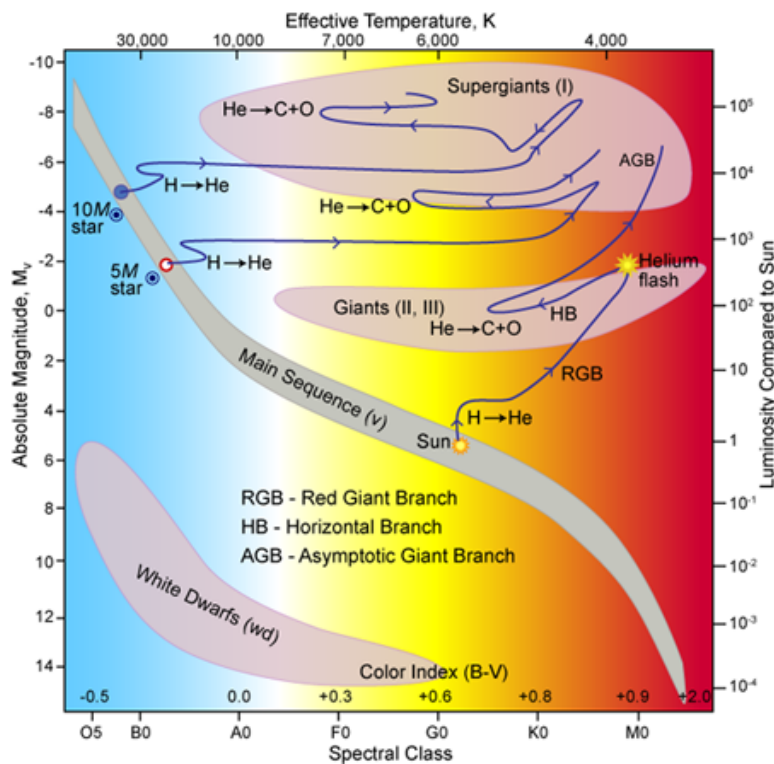
# Contents

<b>INTRODUCTION.....</b>	<b>2</b>
About HR Diagrams.....	2
Introduce M6 and M13.....	3
Importance of the Project.....	5
<b>METHODS.....</b>	<b>6</b>
Observational Methods: data collection.....	6
Theoretical Methods: color index and magnitude.....	8
<b>RESULTS.....</b>	<b>9</b>
Image Analysis.....	9
Photometry.....	13
Preliminary HR Diagrams.....	14
Reference Stars Calibration: final HR Diagrams.....	15
Error Analysis.....	18
<b>DISCUSSION.....</b>	<b>18</b>
M13.....	18
M6.....	19
<b>REFERENCES.....</b>	<b>20</b>

# INTRODUCTION

## About HR Diagrams

Depending on the mass of each star, every star goes through specific evolutionary processes implying their internal structure and energy production which can be reflected by the luminosity and temperature relationships. (Brodie, 2022) Also known as color-magnitude diagrams, **Hertzsprung–Russell (HR) diagrams** depict the relationships between the apparent or absolute magnitudes and temperatures of a collection of stars. As exemplified below, these diagrams not only tell us about the color (denoted as **spectral type** in the plot) and magnitude of individual stars, but also, by recognizing patterns, can help us categorize stars in groups. It's by far one of the most useful tools in the study of stellar evolution. Hence, by determining the positions of the stars in the HR diagrams, we can tell in which evolutionary stage they are.



Example HR diagram for various stages of stellar evolution. The blue lines show three different evolutionary scenarios

for stars of 1 solar mass, 5 solar masses, and 10 solar masses as they move from hydrogen burning, to helium burning, and beyond. ( R. Hollow, CSIRO.)

It should be noted that the difference between apparent and absolute magnitudes can affect our judgment due to the inverse square law of flux scale we observe. The difference between the apparent and absolute magnitude denoted via:

$$\mu = m - M \quad (\text{Lubin, 2022})$$

called the **distance modulus**, encodes the information of the distance between us and the object. Thus, a random set of stars will not show any nice pattern, because their apparent magnitude isn't purely related to their luminosity; it also depends on distance. That's the reason why we choose clusters of stars as our observational objects, created in the same cloud of molecules at about the same time, the stars are nearly the same distance from us, so their apparent magnitude is in fact proportional to their luminosity, and hence we can find the growth pattern and characteristics of the cluster of star.

### Introduce M6 and M13

We choose two representatives from each category of clusters – M6 for **open cluster**, and M13 for **globular cluster**. The differences between two categories are summarized in the chart following. First, some statistics about both clusters.



**Messier 6** (M6 also known as the Butterfly Cluster) is an open or galactic cluster of ~120 stars in the constellation of Scorpius. It has an integrated visual brightness magnitude of 4.2.(Wu 2009) The brightest member is BM Scorpi (a K-type orange giant star) of variable magnitude from 5.5 to 7. M6 is estimated to be 94.2 million years old and 0.487 kpc from us. (Wu 2009)

Messier 6 (NGC 6405) image. The brightest star, BM Scorpii, contrasts sharply with its blue neighbors in photographs. (G.Donatiell)

**Messier 13** (M13) is a globular cluster of several hundred thousand stars in the constellation of Hercules. It's one of the best-known clusters of the Northern Hemisphere which has an integrated apparent magnitude of 5.8. (Garner 2017) The brightest star is the variable star V11 (a red giant) of magnitude 11.95. M13 is estimated to be 11.66 billion years old and 6.8 kpc from us. (Garner 2017) Because of the densely packed population,



there are new stars produced from collision, and those newly formed, young stars, known as "blue stragglers", are particularly interesting to astronomers. (Garner 2017)

M13 image: blue newly formed stars are especially luminous. (Sid Leach/Adam Block/Mount Lemmon SkyCenter)

Differences between the open and globular clusters are summarized here in a table, and we wish to see the difference in our HR diagrams.

Open Clusters	Globular Clusters
loosely bound	stable, tightly bound
few tens to a few hundred stars	tens of thousands to millions of stars
found in spiral and irregular galaxies	found in any type of galaxy
wider range of ages and temperatures (mostly blue)	older, redder stars
near Milky Way	all over sky
easier to observe individual stars	more challenging to observe individual stars

## Importance of the Project

Once we have our completed HR diagram, we can analyze the patterns to learn more about our cluster. We can deduce which stars are the main sequence, red/blue giants, and dwarves just by looking at their locations on the graph. Going back to the example HR diagram, the 3 main regions correspond to different evolution phases of stars and the distribution on those of the cluster has the information of the age of the overall cluster.

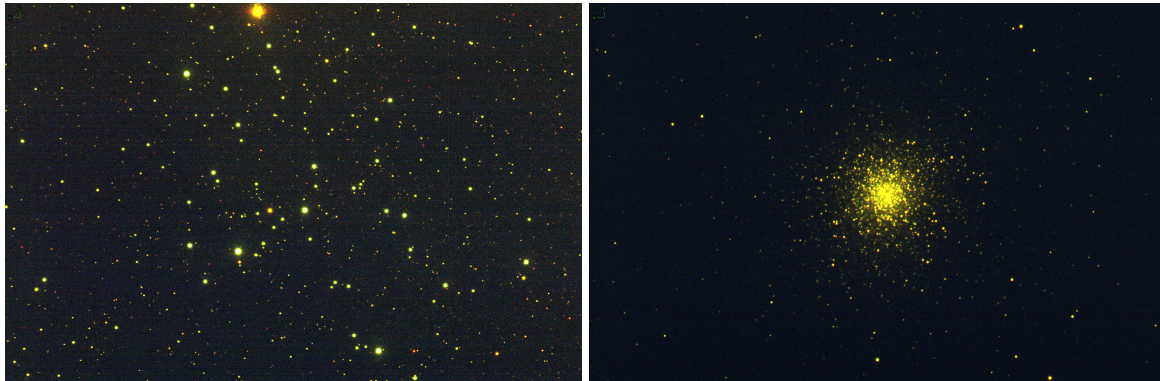
This is based on the nuclear fusion in stars. The color indices (usually B-V) or spectral type representing temperatures have the relative scale from left (hot) to right (cool) since the bluer the hotter, and the apparent magnitude has the scale from top (luminous) to bottom (dim). The **main sequence** stretching from the upper left to the bottom right dominates the population of stars in the HR diagram. It is here that stars spend about 90% of their lives burning hydrogen into helium in their cores. (Brodie, 2022) **Red giant stars** are formed once they have exhausted the hydrogen fuel in their cores and have started to burn helium and other heavier elements. In a typical cluster, formed at the same time, at first stars were all located along the main sequence by mass, lower-mass stars at the lower right. Over time higher mass stars have evolved off the main sequence into red, then blue giants and beyond. (Nemiroff & Bonnell, 2019) **White dwarf stars** (luminosity class D) are the final evolutionary stage of low to intermediate-mass stars and are found in the bottom left of the HR diagram. These stars are very hot but have low luminosities due to their small size. (Brodie, 2022)

With that knowledge, we can look at the color at which the stars tend to become red giants, known as the turnoff point. That will tell us about the age of the cluster as redder turnoff points correspond to older clusters. Furthermore, we can compare the shapes and trends between our diagrams of M6 and M13 to analyze how they differ based on the type of cluster and see if it aligns with the characteristics of open and globular clusters. And that's the core of our comparison study. In the bigger picture, by experimentally comparing the ages of clusters in the context of stellar evolution, we can repeat the procedure for many other clusters at different redshifts. That way, we gain knowledge of the Reionization history, which tells the story of when the galaxies and quasars first started to form due to the ionization of neutral primordial gas (hydrogen and helium).

## METHODS

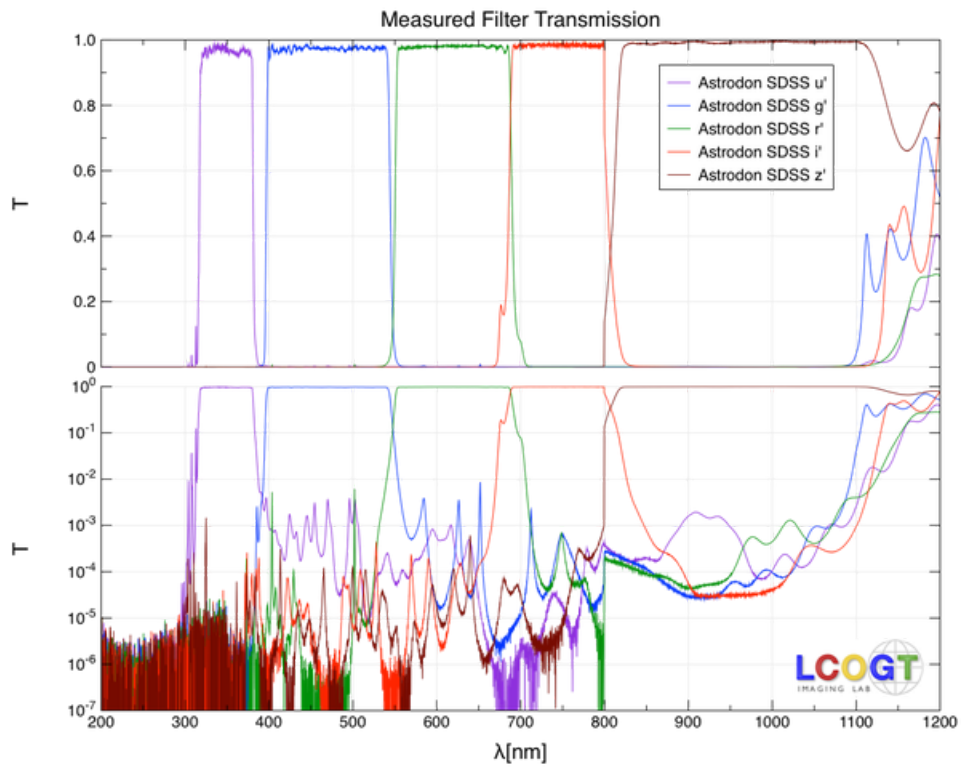
### Observational Methods: data collection

The telescope we are requesting observation from is the LCO's SBIG STL-6303 0.4m telescope with filters Sloan u', g', r', i', Johnson-Cousins B, V, Pan-STARRS w, z\_s. (LCO) By requesting 1s, 10s, and 100s integration time for 10 exposures each for M6 and 10s, 100s integration time for 10 exposures each for M13 (since it's slightly dimmer) in SDSS i, g, r, u filters, we are able to decide which images of both clusters to use for preprocessing with AstroArt 8. We first only requested 10 s for each SDSS filter and found that the color images are not ideal as we can see below.



Preliminary color images of M13 and M6 with aligned images in SDSS g, r, u filters for the RGB coloring.

The hypothesis is insufficient integration time on the g band, so we requested multiple integration times and decided to use the 10s exposure time after confirming that they had no irregularities, such as streaking, satellite traces, or noisy readouts. With AstroArt 8, we aligned all of the images for each filter using the average function. This ensures that signal outliers are averaged out. We used these aligned images in all bands for all further analysis. The final color images are synthesized based on the responses of the SDSS filters as shown below.



Sensitivity functions of the SDSS filters  $u'$ ,  $g'$ ,  $r'$ ,  $i'$ ,  $z'$ . (LCO)





Final color image plus aligned images in filters we use.

### Theoretical Methods: color index and magnitude

We define the color index of an object in two filters by the difference in magnitude of that object as measured in the two filters. (Lubin, 2022) Assuming all the stars are approximately perfect blackbodies, the color is directly related to the temperature of the object. (Lubin, 2022) Therefore, our HR diagrams will have the effective temperature represented with a color index on the x-axis and an apparent magnitude on the y-axis. For example, the U-B color index is:

$$U - B = -2.5 \log \left( \frac{\int d\lambda S_U(\lambda) F_\lambda}{\int d\lambda S_B(\lambda) F_\lambda} \right) + C_{U-B} \quad (\text{Lubin, 2022})$$

, where  $C_{U-B}$  is the difference of zero points in U and B filters. By reading off the response of SDSS filters and based on the quality of acquired images in each band, we have decided to use g-r color index to denote the temperature axis of HR diagrams. Going back to the SDSS filters response diagram above, the smaller the g-r color index is (the more left on the axis), the hotter the object is.

Reminding that the conversion between flux and apparent magnitude is through:

$$m_1 = m_0 - 2.5 \log \left( \frac{f_1(\lambda)}{f_0(\lambda)} \right) \quad (\text{Lubin, 2022})$$

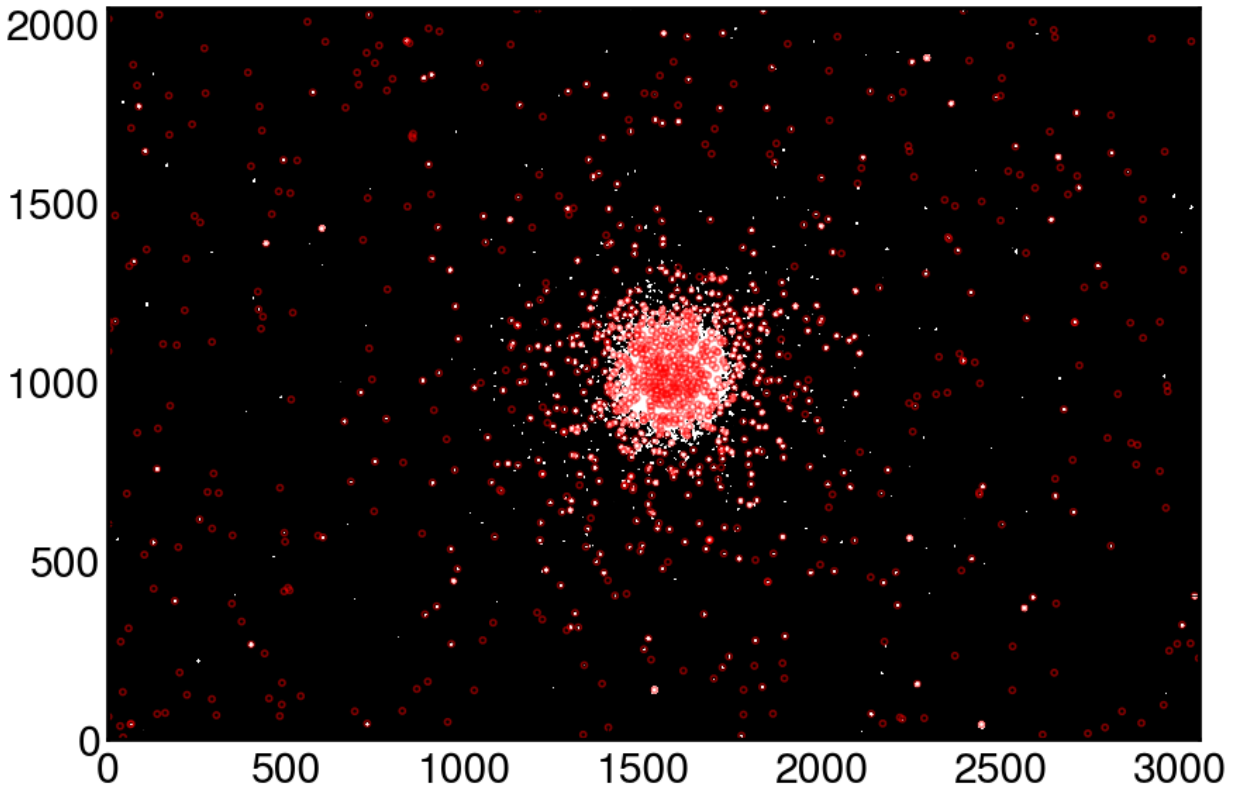
, where  $f(\lambda)$  is the sky-subtracted flux in the aperture or of the star and  $m_0$  is the known magnitude of the reference star. We need a reference star for calibration from instrumental magnitude to the apparent magnitude. For accuracy, we plan to use five reference stars for each cluster and apply curve fit to find the magnitude zero point in each filter. The apparent magnitude (y-axis) is represented by g-band magnitude for consistency with the g-r color index. This doesn't lose the generality of the luminosity of stars for the same reason of closely spatially correlated stars in clusters as mentioned previously.

## RESULTS

### Image Analysis

We opened the g-band preprocessed and aligned .fits file exported from AstroArt 8 with *astropy.io.fits* function. We first need to subtract the background signal added to the perfect image by electronic bias, dark current, cosmic rays, and any other signal that doesn't come from an astronomical source. (Burns, 2022)

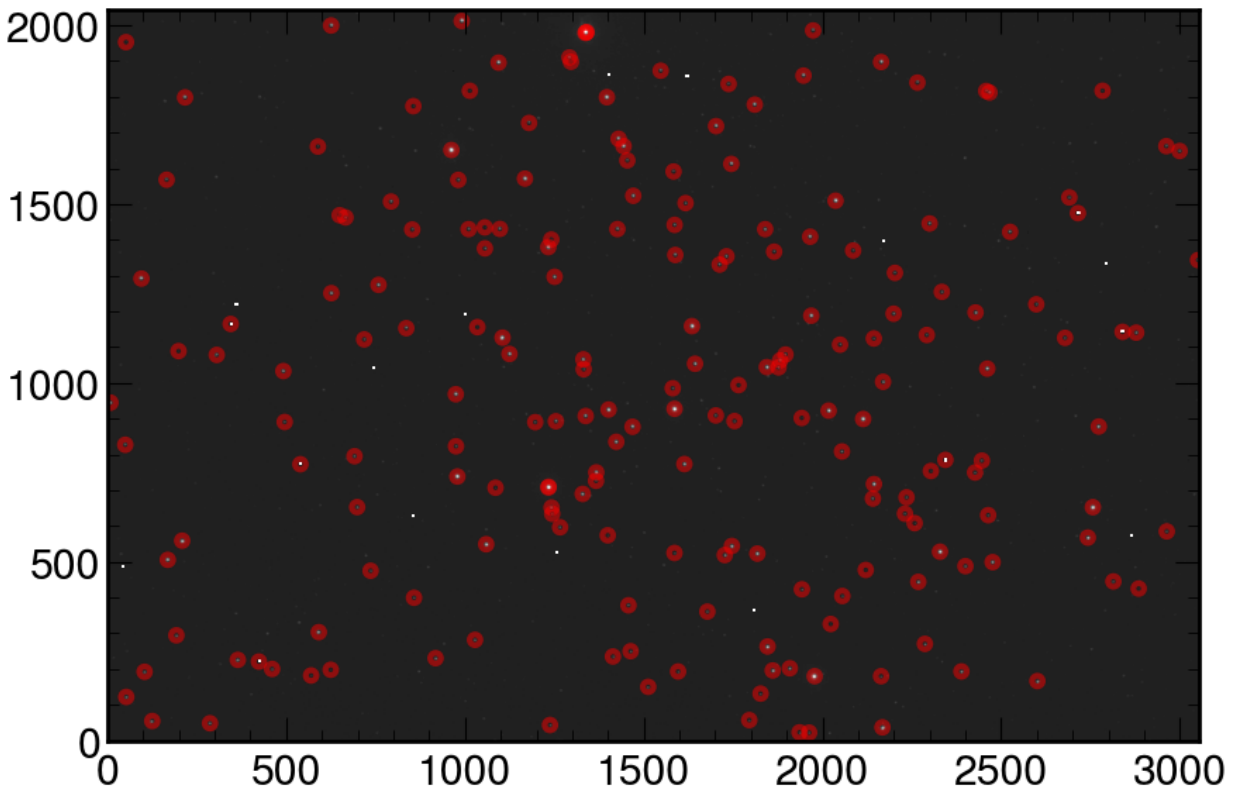
The standard method for sky background estimation uses three-sigma clipping to filter out the flux outside the three-sigma range and compute the mean or median of the background signal again. This way removes contaminations and bad pixels. We apply this with the *photutils* library, together with *photutils.detection.DAOSStarFinder* for locating the centroids of stars after sigma-clipped background, we have the first source finding images for M13 and M6 as shown below.



id	xcentroid	...	flux	mag
1	43.79695981035774	...	1.064501166343689	-0.06786535404682248
2	1773.707986455734	...	21.894123077392578	-3.3508188878331175
3	1330.8923957974564	...	1.0511635541915894	-0.05417573668491892
4	2616.0557472381	...	1.0570448637008667	-0.0602335506816252
5	2742.806198262361	...	2.348836898803711	-0.9271321519814696
6	1401.2362838341917	...	1.0249907970428467	-0.02679991515881915
...	...	...	...	...
1159	732.2703620550558	...	3.0458528995513916	-1.2092723127858749
1160	144.90507974995387	...	1.159446120262146	-0.1606264291868003
1161	1835.0590967044193	...	3.653639793395996	-1.4068143217917164
1162	2394.9260339815037	...	38.575721740722656	-3.965785150841914
1163	1145.0488902332618	...	1.0625684261322021	-0.06589226712297469
1164	1204.752859361718	...	5.142759799957275	-1.7779906011054565

Length = 1164 rows

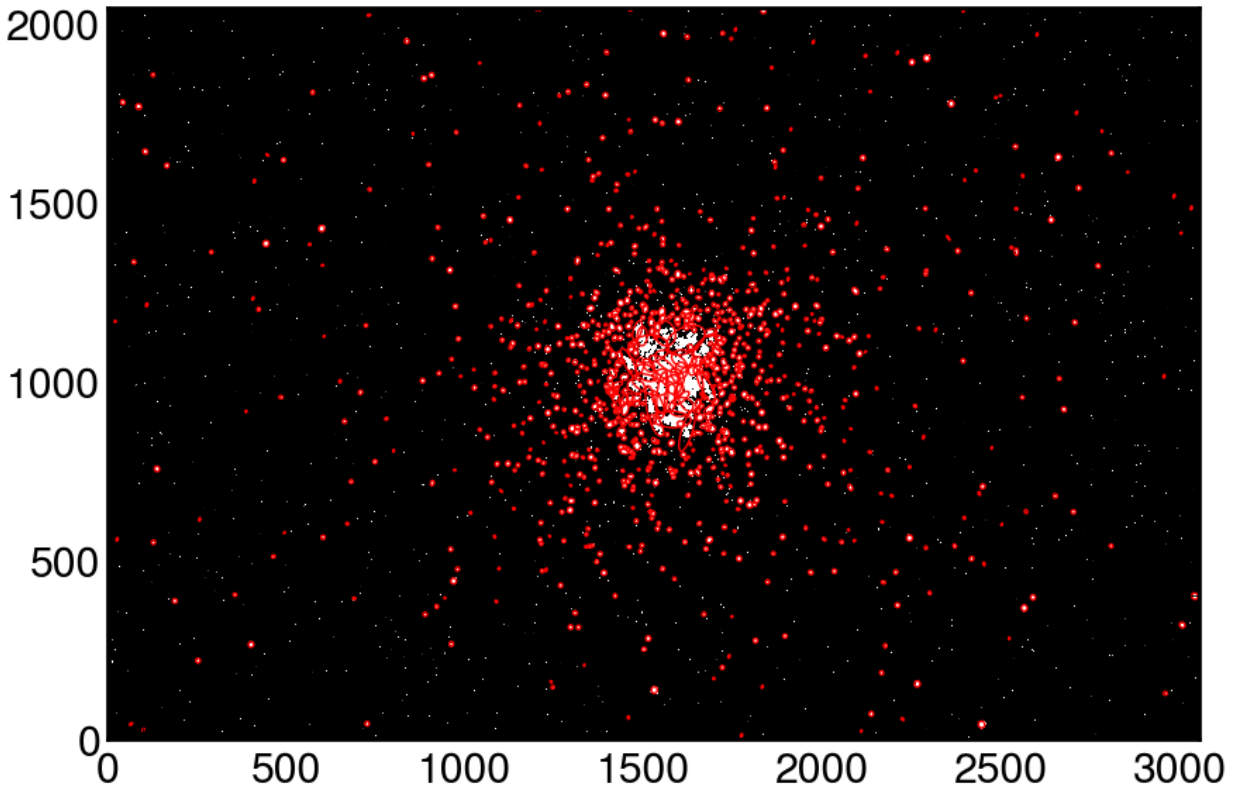
DAOStarFinder source finding results for M13



DAOStarFinder source finding results in logarithmic plot for M6

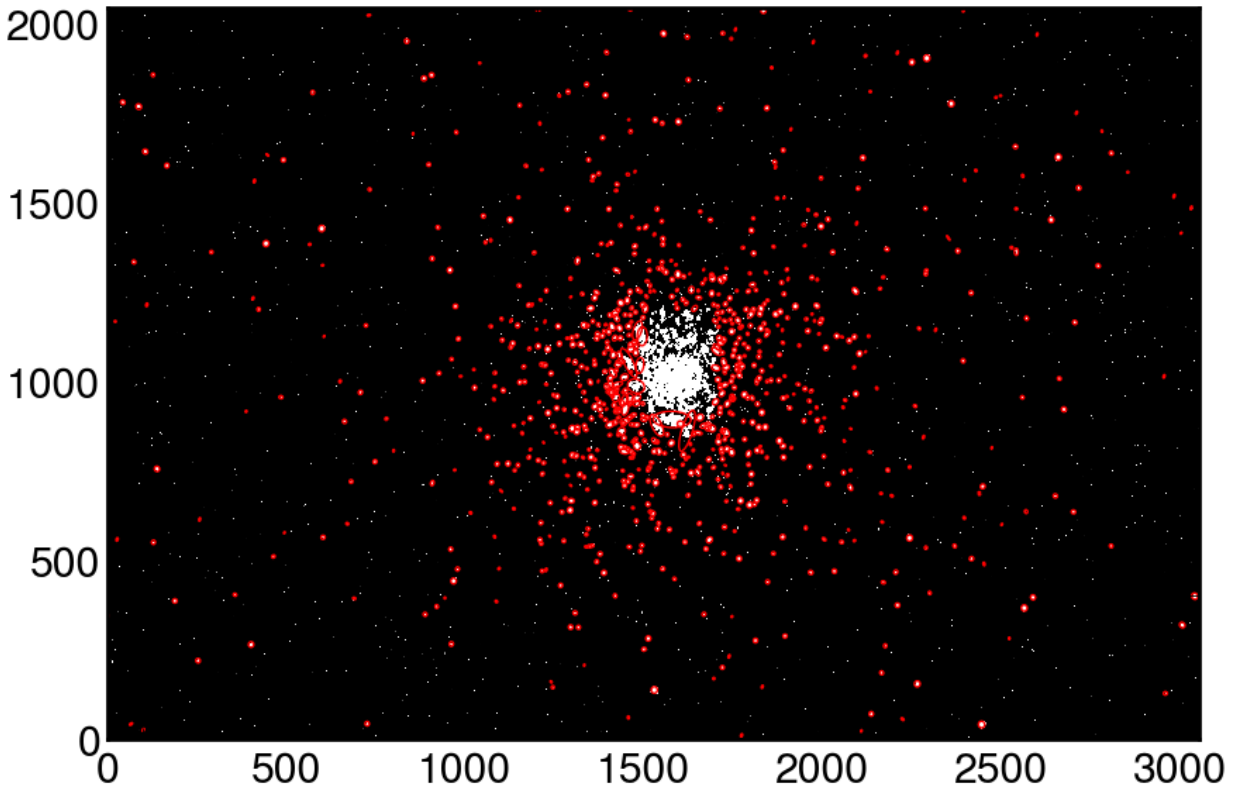
Notice that the mean flux per source in M13 for example is very low ( $\sim 1.49$ ) and, in the logarithm plot, many sources were not picked, the star finder is picking out many noise points or background and foreground instead of astronomical objects in the M13 cluster. We deduced that it results from the LCO telescope itself having already done noise reduction, so further clipping would make the irrelevant objects more dominant.

We hence switched to Python library for *Source Extraction and Photometry (sep)*. The *sep.Background()* function allows us to compute the representation of spatially variable image background and noise instead of averaging over pixels. This effectively eliminates the noise and irrelevant signals. The following image and table show the newly found sources. We can see the number is significantly reduced and less noise/stars not in M13 is captured.



SEP extractor source finding results

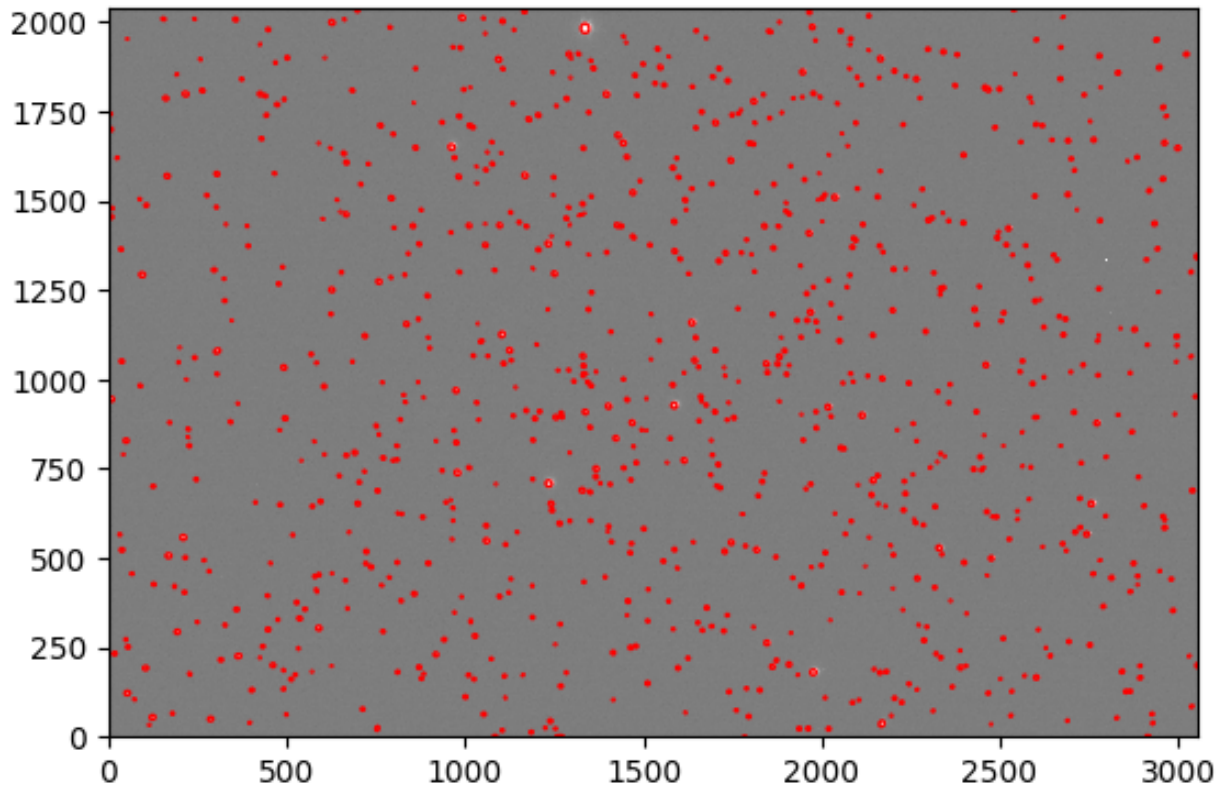
But what is concerning is the low resolution at the center of M13 due to the highly dense population has resulted in inaccurate star selection. There are many techniques to perform photometry for such a compact or unresolved area, but in order to improve the signal-to-noise ratio (SNR), we decided to mask this area. The residual sources are sufficient for the purpose of this research. And we need to make sure all selected sources both exist in g and r filters, we do so by filtering out all negative flux sources in r-band (details see our *photometry()* function in M13 notebook in GitHub). So the final source extraction after masking looks like the following image and table, and M6 doesn't have this problem as an open cluster.



id	xcenter pix	ycenter pix	aperture_sum
1	1773.8860497803646	8.655002132728766	2191.3972661986863
2	2108.9345720506103	21.26586844770829	380.24146961597165
3	726.4954735824375	41.458628390338795	1838.5297837768076
4	2445.408312308892	39.08337130993737	65850.52619586112
5	2224.3255159799505	54.16974111533244	627.4551725206477
...	...	...	...
818	1756.8246950569546	1982.4365660219028	902.4778099665276
819	731.3125365854435	2022.3370800722635	621.2878718092473
820	2394.728723141711	2034.9790941655847	2475.4084349748982
821	1204.777901040581	2038.9755869156668	2773.784916674254
822	1460.9782066452392	2038.5328449241524	763.314027084027
823	1835.1697889940301	2034.7200933281276	5089.161182318099

Length = 823 rows

SEP extractor source finding results after masking M13



SEP extractor source finding results for M6

### Photometry

We will measure the luminosity of star-like sources with a point spread function (PSF) that is approximately Gaussian shape. By simply adding all of the signals in a circular region or aperture around the star’s center after background subtraction, we perform the procedure called **aperture photometry**. Now, with the source extractor, we already have the center of the Gaussian PSF (x-centroids, y-centroids) in pixel coordinates. By defining the aperture to have a radius of 5 pixels with the *CircularAperture* function, we can use *aperture\_photometry* function, to sum up the analog to digital units (ADU) in each aperture. The relationship between the intensity of the star we measure in ADU as  $f(\lambda)$  and the actual flux of the star  $F(\lambda)$  in electrons is just:

$$f(\lambda) = c(\lambda)F(\lambda) \quad (\text{Lubin, 2022})$$

, where  $c(\lambda)$  is a “constant” that depends on the specifics of our telescope, filter, CCD, etc. Here, we use the gain of our telescope as shown in the chart to convert between units.

# ■ ■ ■ SBIG STL-6303

Format	3Kx2K 9-micron
FOV (arcmin)	29.2 x 19.5
Pixel size (1x1 binning, arcsec)	0.571
Default binning	1 x 1
Cycle time (readout+overhead; 1x1 binning, s)	14 s
Read noise (e-)	14.5
Gain (e-/ADU)	1.6
Dark current (e-/pix-s)	0.03 @ -100 C (estimated)
Filters	Sloan u', g', r', i', Johnson-Cousins B, V, Pan-STARRS w, z_s

## LCO's SBIG STL-6303 0.4m telescope statistics. (LCO)

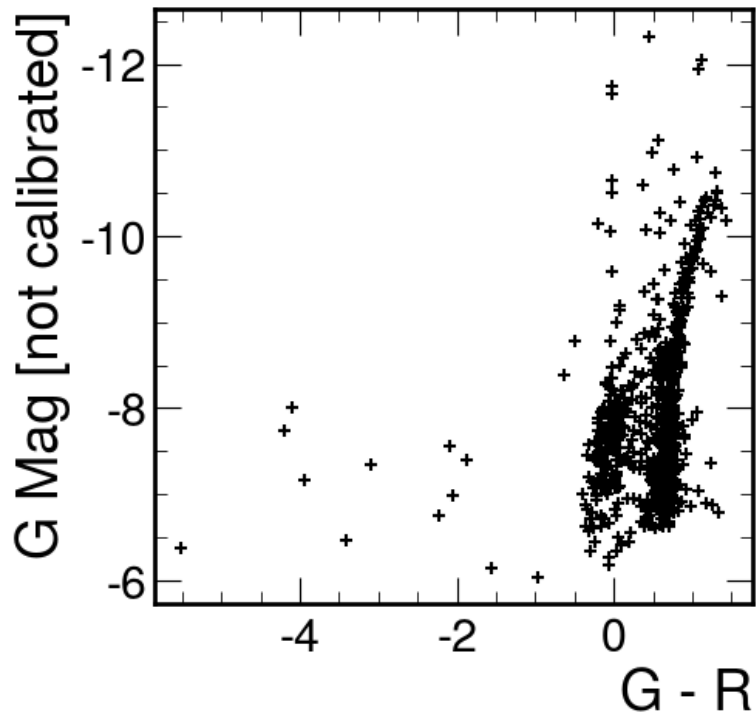
For comparative photometry, we have the equation

$$m_1 - m_2 = -2.5 \log \left( \frac{\mathcal{F}_1(\lambda_1)}{\mathcal{F}_2(\lambda_2)} \right) = -2.5 \log \left( \frac{f_1(\lambda) / c(\lambda)}{f_2(\lambda) / c(\lambda)} \right) = -2.5 \log \left( \frac{f_1(\lambda)}{f_2(\lambda)} \right) \quad (\text{Lubin 2022})$$

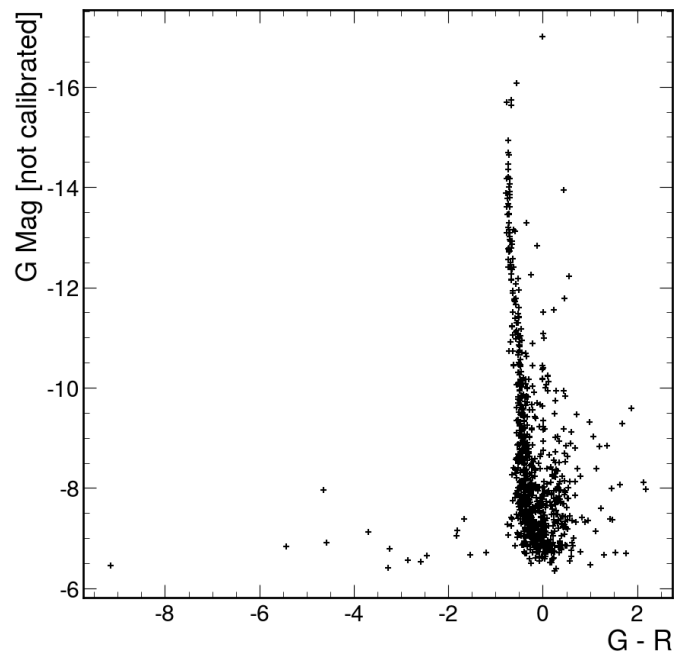
So the constants for the same band cancel out.

## Preliminary HR Diagrams

Computing the magnitude with the converted ADU to  $e^-$  aperture integrated flux, we can hence plot the preliminary HR diagram with the g-band and r-band magnitudes before zero point calibrations.



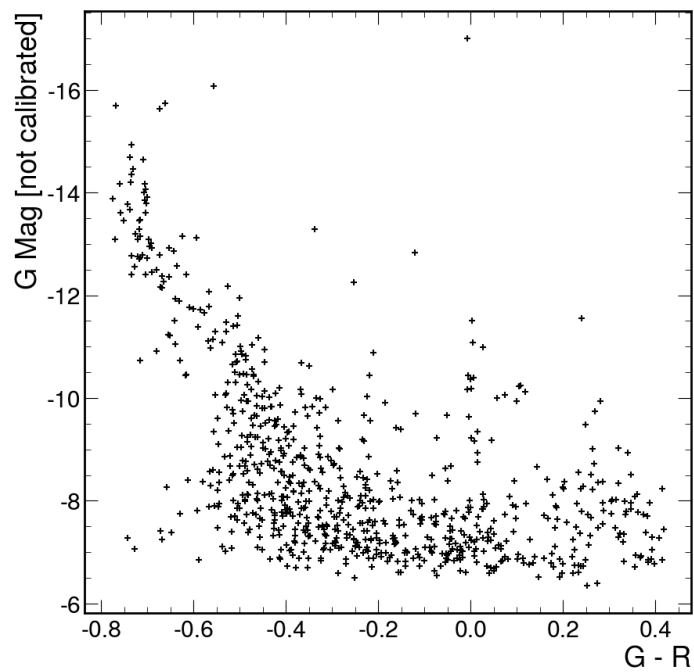
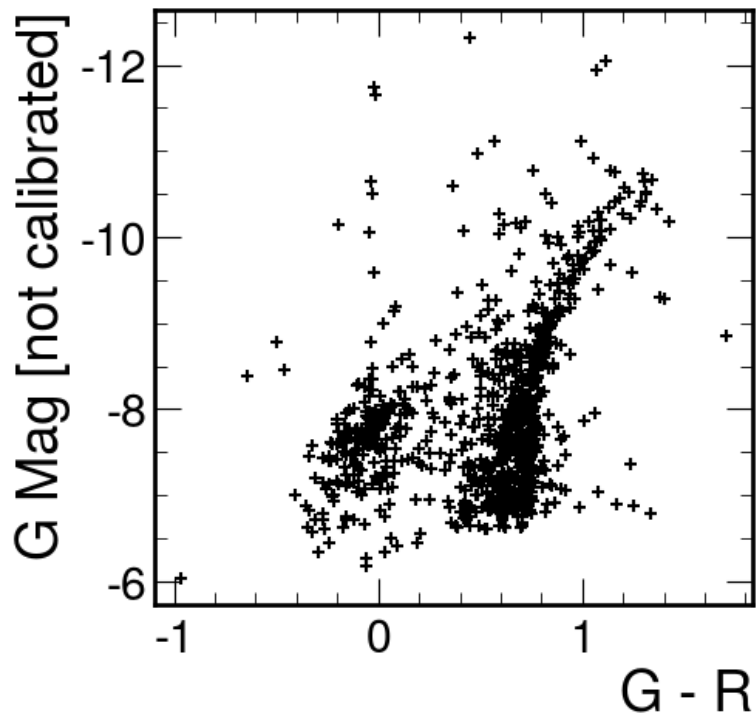
First HR diagram for M13



First HR diagram for M6

It's obvious that there are some abnormally hot outliers on the left end of the plot. We

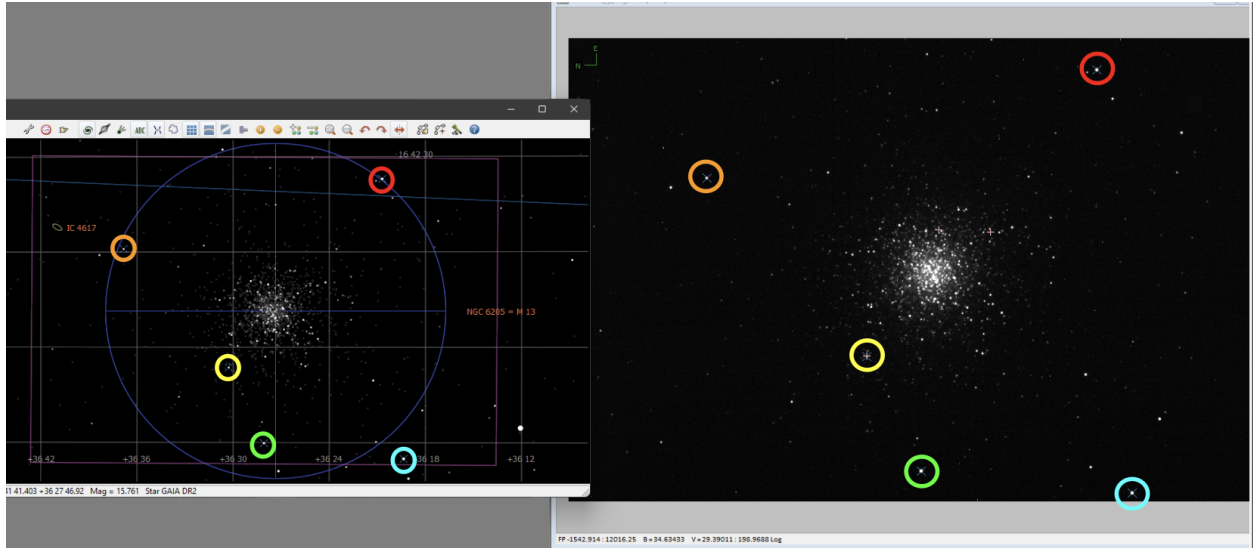
then apply a three-sigma clipping to eliminate the outliers that might result from some large leftover patch of unresolved sources from masking.



Preliminary HR diagram for M13 and M6 after sigma-clipping

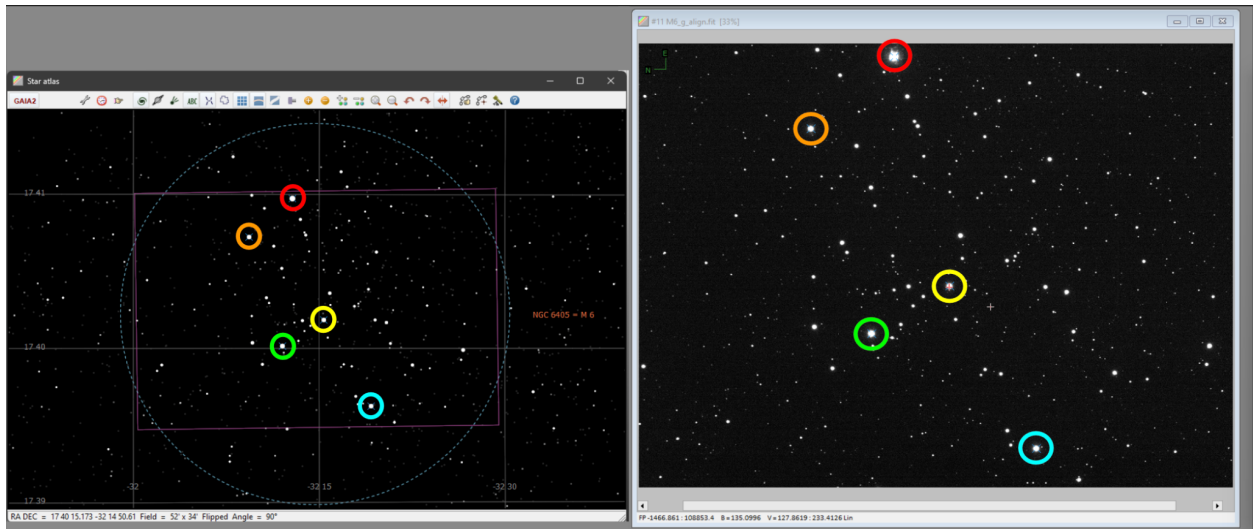
## Reference Stars Calibration: final HR Diagrams

The last step is to do the calibration with chosen 5 reference stars and their known magnitude as described in the Methods section. We use the Star Atlas tool on AstroArt to extract the reference star information. So for M13, we have the following stars chosen to match those on the database image after proper rotation.



RA(hour, min, sec)	Dec (degree, min, sec)	Apparent Magnitude
16 40 54.9	+36 19 22	10.17
16 40 59.7	+36 28 04	10.60
16 41 23.5	+36 30 17	11.52
16 42 01.1	+36 36 51	11.66
16 42 22.9	+36 20 43	10.34

Reference stars for M13

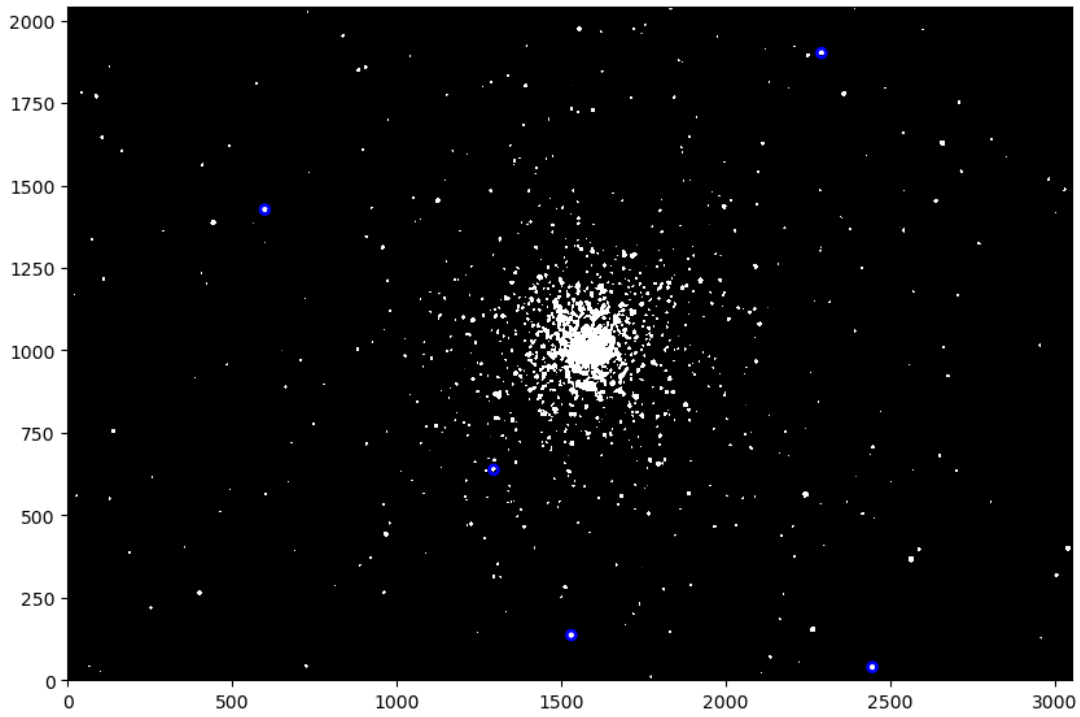


RA(hour, min, sec)	Dec (degree, min, sec)	Apparent Magnitude
17 39 37.6	-32 19 13	7.12
17 40 01.0	-32 12 04	6.70
17 40 11.1	-32 15 24	7.21
17 40 43.4	-32 09 21	7.21
17 40 58.5	-32 12 52	5.24

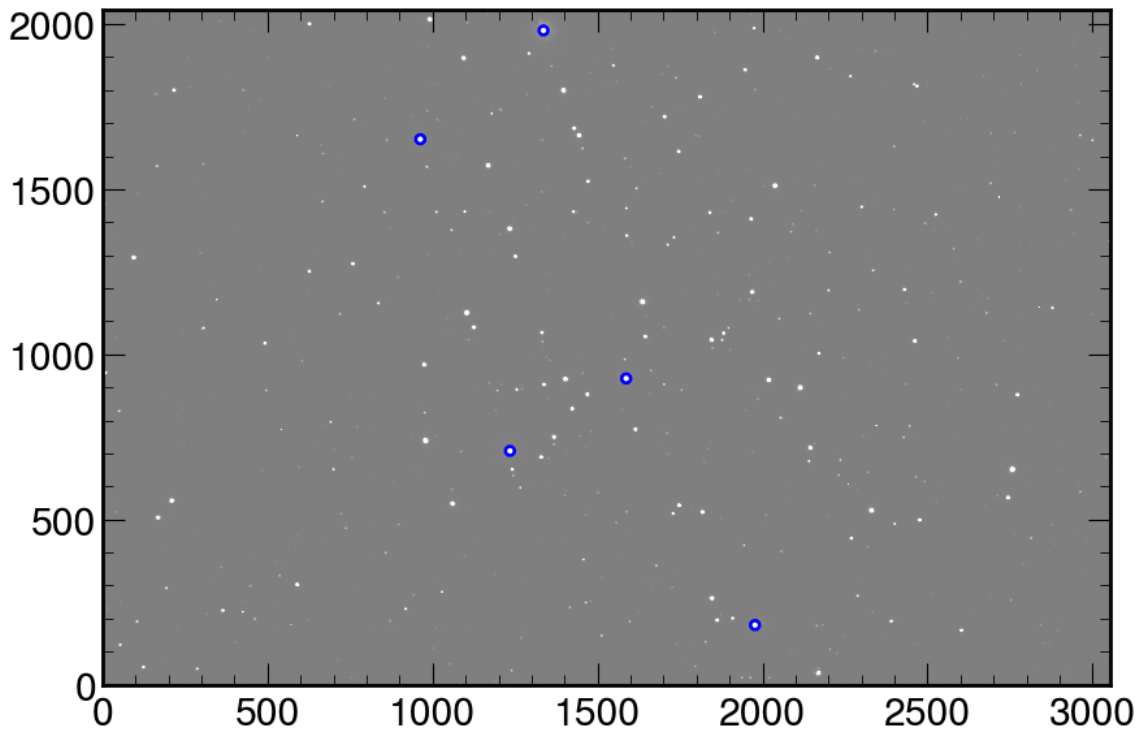
Reference stars for M6

The corresponding sky coordinates and magnitude are summarized in the charts.

By using *Angle* and *skycoord\_to\_pixel* functions in the *astropy* library, and the World Coordinate Systems (WCS) information retrieved from the .fits files, we have located the reference stars in terms of pixel coordinates as what we have extracted for centroids of sources. These thus can be plotted.



Reference stars in pixel coordinates for M13

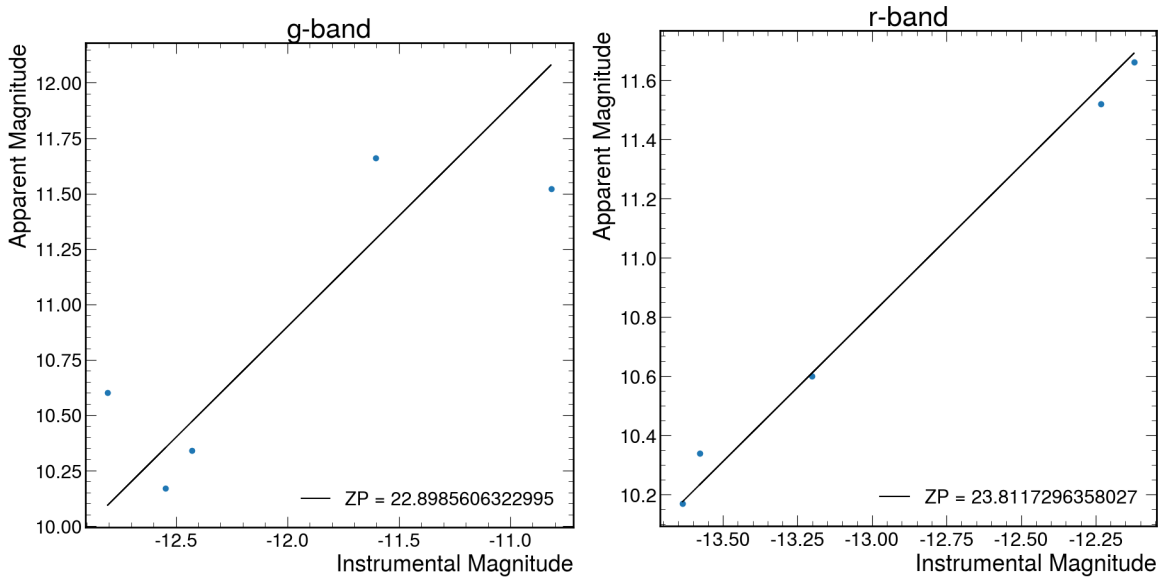


Reference stars in pixel coordinates for M6

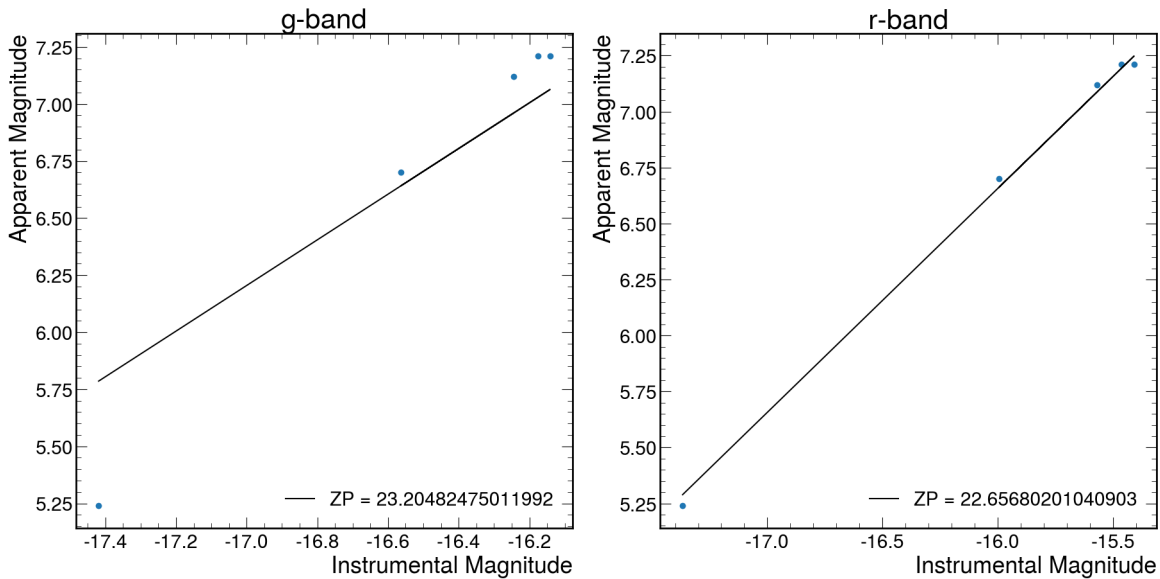
This way we follow the same aperture photometry procedure for these five PSF centers. The same formula from comparative photometry applies here except the  $m_0$ ,  $f_0$  now denotes the reference stars calibration which should be constant for each filter.

$$m_1 = m_0 - 2.5 \log \left( \frac{f_1(\lambda)}{f_0(\lambda)} \right) \quad (\text{Lubin, 2022})$$

So we can use least-square regression linear fitting to find zero points of each filter.

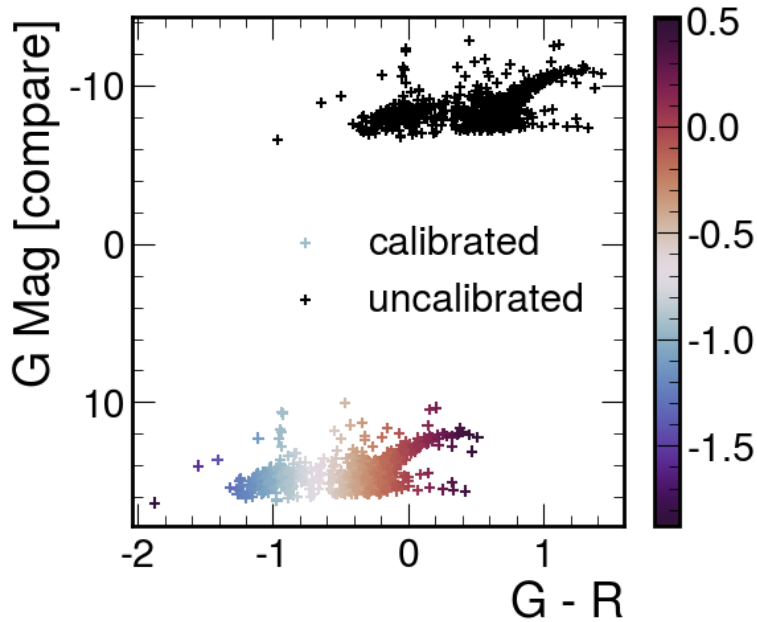


Zero point fittings in g and r bands in M13

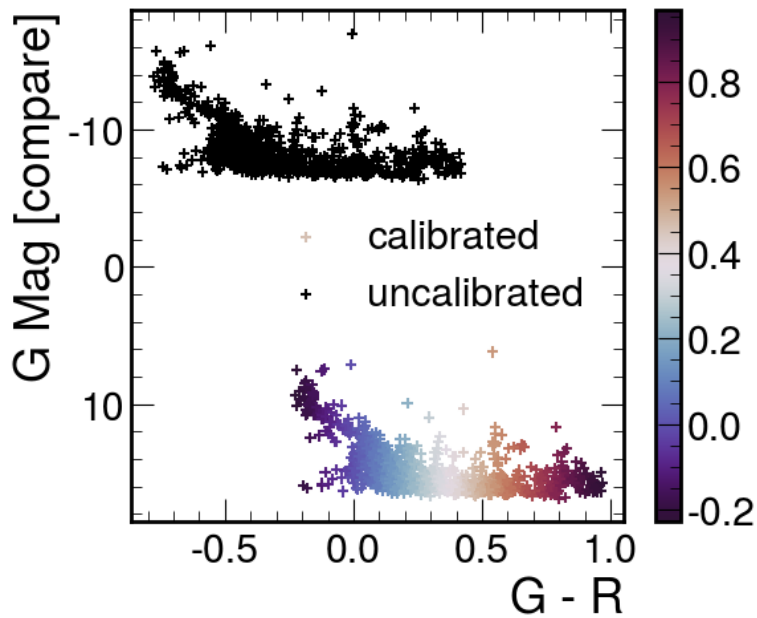


Zero point fittings in g and r bands in M6

By adding  $C_{g-r}$  the difference of zero points in g and r filters to the preliminary g-r color indices, we have the calibrated g magnitude and color index. The translation in the HR diagram is significant.



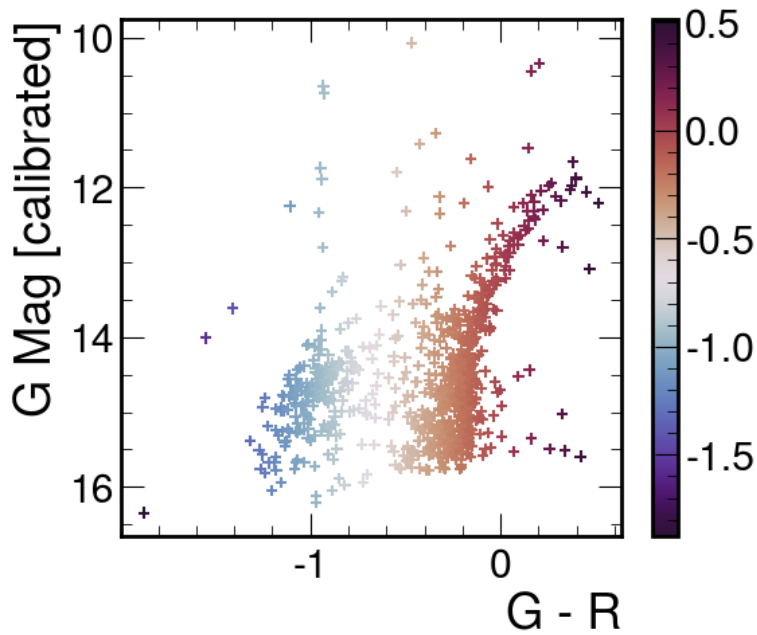
Translation from uncalibrated to calibrated magnitudes for M13 HR diagram



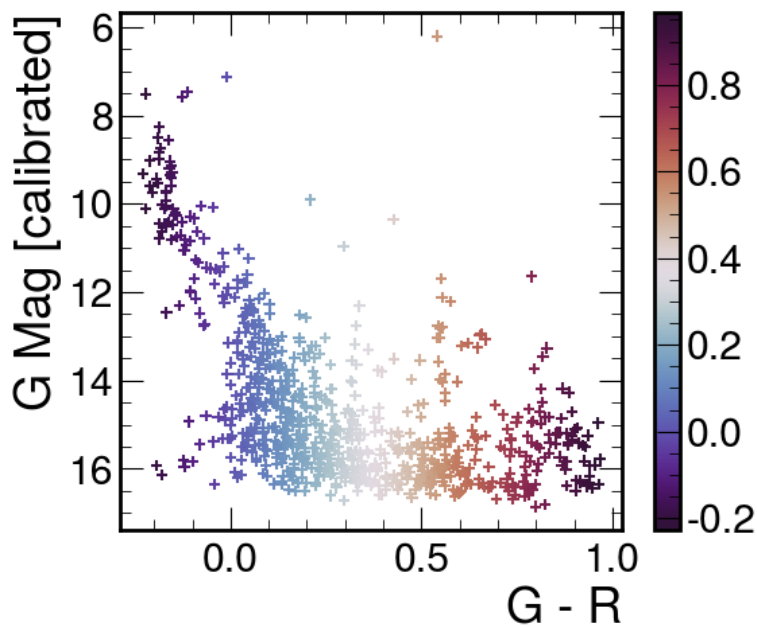
Translation from uncalibrated to calibrated magnitudes for M6 HR diagram

Now the magnitudes in M13 make more sense falling under the brightest star V11(a red

giant) magnitude 11.95 (the y-axis is reversed for smaller magnitude brighter the star is). Same for that pf M6 falling under the brightest star BM Scorpi of variable magnitude from 5.5 to 7.



Final HR diagram for M13



Final HR diagram for M6

## Error Analysis

There are many sources of errors in measurement experiments like this. According to the lecture notes, we need to at least consider the systematic/instrumental noise from the telescope (readout Noise, dark current) and measurement noise (background noise, source output noise). (Lubin, 2022) The signal-to-noise ratio (SNR) is expressed compactly in one equation:

$$SNR = \frac{S}{N} = \frac{S}{\sqrt{\sigma_R^2 + \sigma_{dc}^2 + \sigma_\beta^2 + \sigma_S^2}}$$

where  $\sigma_R^2$ ,  $\sigma_{dc}^2$ ,  $\sigma_\beta^2$ ,  $\sigma_S^2$  to denote for readout noise, dark current, background noise, and signal output uncertainty respectively. The first two are instrumental-dependent so are constant for all filters and sources. The signal  $S$  is the total flux in electrons integrated in apertures, so it's different for each star-like object. By assuming a Poisson probability distribution of the stochastic output from *aperture\_photometry* and *sep.Background* functions, the uncertainties for signal and background are simply the square root of the aperture flux sum and the square root of the background signal. (Narbutis et al., 2015) Even if we have subtracted off the background signal, we are still left with some noise due to the random distribution of the noise, so we still need to take the background signal uncertainty into consideration. (Lubin, 2022)

Other things that add to the noise are the uncertainty we have for curve fitting in reference star calibration and the quantum efficiency of CCD image sensors for different wavelengths and hence filters.

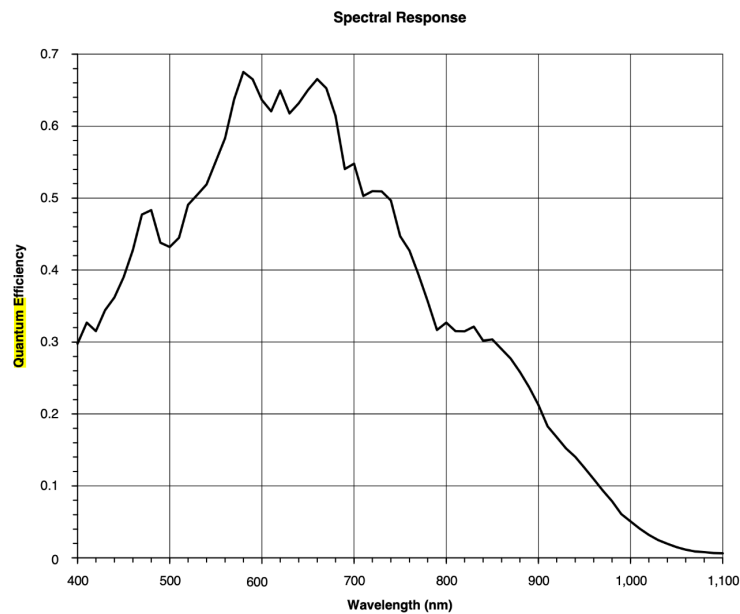
All the formulas and values of sources of noise are expressed in the table below.

Source of error	Value/Equation
Readout noise	14.5 e <sup>-</sup>
Dark current	sqrt(0.03) @ -100 C (estimated) e <sup>-</sup> /pix-s
Background estimation	$\sigma_S = \sqrt{\pi \cdot r_{pho}^2 \cdot \mu_{bkg}}$ (Narbutis et al., 2015)

Photon counts	$\sigma_S = \sqrt{S}$
Curve Fit	Residual mean for zero point fitting
Quantum Efficiency	$S = F\tau A\epsilon Q_e$ (Lubin, 2022)

### Noise sources estimations

Quantum Efficiency of the KAF-6303 Frame CCD Image Sensor:



Typical Spectral Response (Semiconductor Components Industries, LLC, 2015)

The CCD image sensor has a maximum quantum efficiency of about 65% at red wavelengths and decreases at smaller wavelengths (~65% for SDSS g and ~40% for SDSS r). As a result, the relative fluxes from each band may not only be from differences in the actual fluxes received by the sensor but also include errors due to the different sensing capabilities at different wavelengths. This is included in the formula

$$\frac{S}{N} = \frac{FA_e\sqrt{\tau}}{\left[\frac{N_R^2}{\tau} + FA_e + i_{DC} + F_{\beta}A_e\Omega\right]^{1/2}} = \frac{FA_e\sqrt{\tau}}{\left[\frac{N_R^2}{\tau} + N_T\right]^{1/2}} = \frac{FA_e\tau}{\left[N_R^2 + \tau N_T\right]^{1/2}}. \quad (\text{Lubin, 2022})$$

Since the residual in linear curve fit is post-processing of magnitude calibration, the uncertainty for it will be added directly to the color index axis in HR diagrams instead of

being included in the SNR function.

Note that these formulas are for computing the SNR of magnitude in one filter, and the color index is computed from the subtraction of g and r band magnitude. From the Propagation of Uncertainty theory, both the uncertainties in magnitude from two filters add up:

$$\sigma_{g-r} = \sqrt{\sigma_g^2 + \sigma_r^2}$$

But to convert from the uncertainty from flux to magnitude, we need to use the conversion formula,  $Mag = -2.5 \log(S) \rightarrow = 2.5 \log(1 + N/S)$ , so after derivation we have:

Error on Mag  $\sim 1/(S/N)$  (Hainaut, 2005)

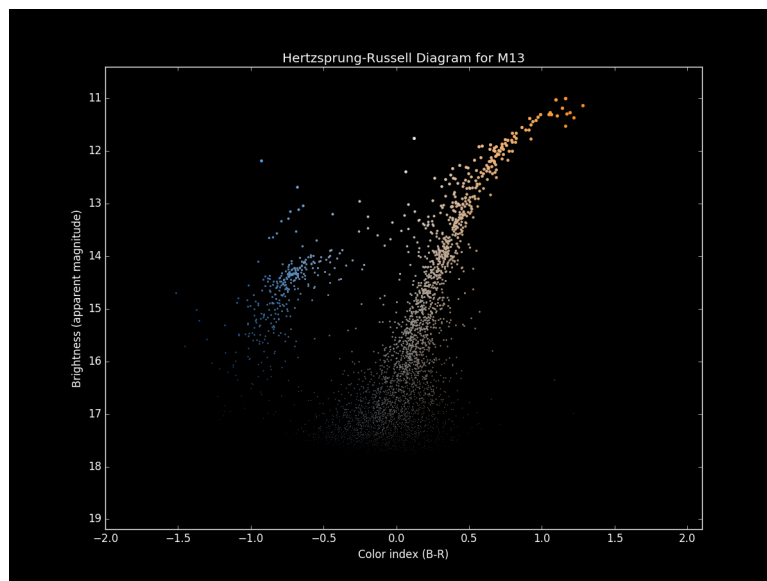
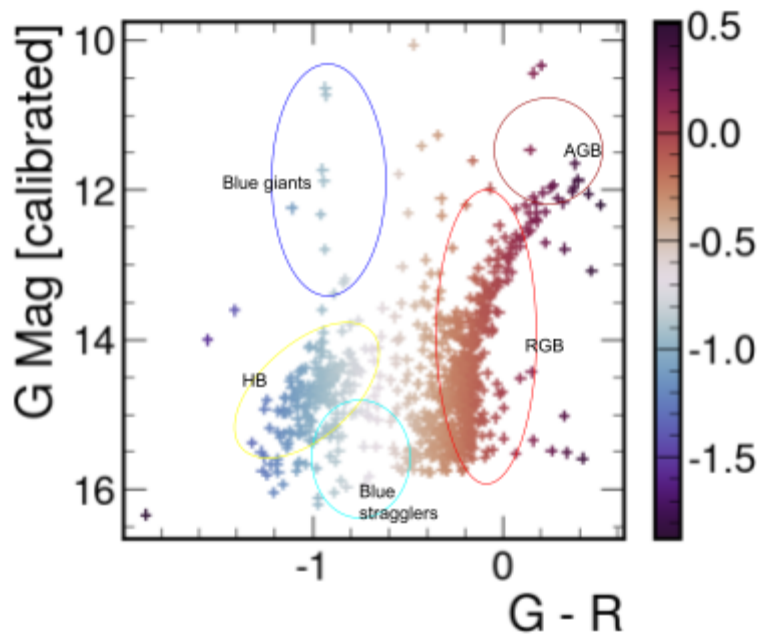
With this knowledge, we can compute the SNR of filter magnitudes and color index for each source and compute the average SNR for the overall cluster.

	M13	M6
SNR - g filter	45.043 or 76.152 dB	79.203 or 87.440 dB
SNR - r filter	57.623 or 81.078 dB	61.567 or 82.402 dB
g-r color index error (mag)	0.0433	0.0558
Zero point fitting - g filter (mag)	-1.066e-15	-2.842e-15
Zero point fitting - r filter (mag)	-1.421e-15	-3.553e-16

The calculated SNRs are good in each filter, so the image analysis we have carried out is unbiased. The color index has less than 10% error in magnitude, so the HR diagrams are within the range of acceptable accuracy.

## DISCUSSION

### M13



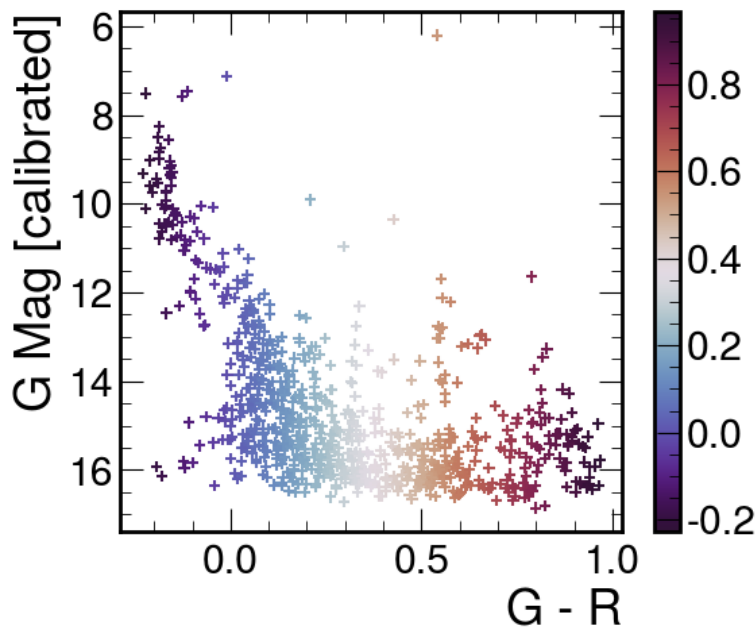
Annotated HR diagram for M13 compared to its reference (Vanderbei)

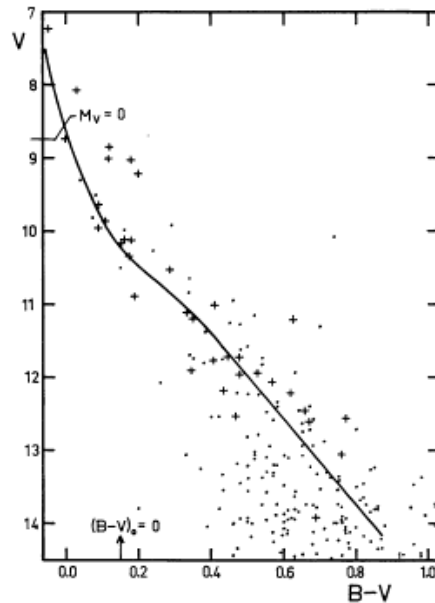
Comparing our final HR diagram with the reference from Gaia Data, we can say that we have the shape and scale right. But compared to a typical HR diagram, what we don't

have is the diagonal main sequence that's supposed to stretch from the right bottom. The major groups we have here are red giants/supergiants (RGB) (upper right), blue giants (upper left), and horizontal branch (HB) stars (lower left).

Stars evolve off the main sequence to the RGB by fusing hydrogen into helium or with a helium-burning shell outside a degenerate carbon–oxygen core, and a hydrogen-burning shell just beyond that for asymptotic-giant-branch (AGB) which is higher up in luminosity in the upper left region. Then the stars fuse helium to carbon in their core going to the HB stars which have reduced luminosity and higher temperature (bluer) due to stellar structure change. Some massive stars develop into blue giants in the fusion process and become high-mass luminous stars, but these are very rare as we can see in the upper left corner of the diagram. The "blue stragglers" that we mentioned in the introduction are shown as the lower gray points in the middle as they are newly born so somewhat hot but not as bright as HB stars because of their relatively small size. But the stars on the red end still dominate the cluster. The very low position of the turn-off from the main sequence to the red giant branch, that we cannot even observe beyond ~16 magnitudes, indicates the cluster's age at about 12 billion years. (Nemiroff & Bonnell, 2019)

## M6





HR diagram for M6 compared to its reference (Vleeming, 1974)

<http://spiff.rit.edu/classes/phys230/lectures/clusters/clusters.html>

When comparing our diagram to the photometric study, we see the general pattern of the main sequence in both diagrams stretching from bottom right to upper left corner. There is no distinct turn off point as seen in the M13 cluster, meaning that most of the stars are still in the main sequence starting from least massive stars on the right. This indicates that this cluster should represent a relatively new cluster.

As we did not have the time or resources to do the clustering analysis, we have referenced a previous work on the cluster (Vleeming, 1974). Other studies have determined the age of this cluster to be around 94.2 million years old (Wu 2009), 100 times younger than M13, which fits the result of a young cluster from the HR diagram.

## Conclusion

We can see that M6 is about 1 magnitude shifted to the right in g-r color index than M13, meaning it's cooler than M13 on average, which makes sense because it hasn't started the higher nuclear synthesis process. But its apparent magnitude is comparable to M13 because it's about 10 times closer to us, with more stars on the blue end for newly born stars compared to the RGB dominated M13. These features all align with the categorization of open and globular clusters as summarized in the first table.

One limitation in both HR diagrams is that there appears to be more stars even in our sigma clipped diagram than the reference diagram. This could also be due to the fact that we cannot determine which stars are actually in the cluster versus stars in between the telescope and cluster or noise that source extractor picked out as a source. This could cause an excess of stars along with the fact that the field was larger than just the cluster so it included other stars. If we could do it differently, we would compare with the existing observations and statistics to sort out the stars that belong to the cluster instead of simply applying sigma-clipping.

## REFERENCES

1. Cover picture: [Tolga Gumusayak](#), [Robert Vanderbei](#)
2. Brodie, J. (2022) Hertzsprung-Russell Diagram: Cosmos, Hertzsprung-Russell Diagram | COSMOS. Available at: <https://astronomy.swin.edu.au/cosmos/h/hertzsprung-russell+diagram> (Accessed: 11 June 2023).
3. HR diagram illustration: Robert Hollow, Commonwealth Science and Industrial Research Organisation (CSIRO), Australia.
4. Philip Lubin (2022) Notes for PHYS 134: Observational Astrophysics (Accessed: 11 June 2023).
5. Messier 6 (NGC 6405) image: [Giuseppe Donatiello](#) from Oria (Brindisi), Italy.
6. Wu, Zhen-Yu; et al. (November 2009), "The orbits of open clusters in the Galaxy", [Monthly Notices of the Royal Astronomical Society](#), 399 (4): 2146–2164, [arXiv:0909.3737](#)
7. M13 image: April 17, 2008, Image by Sid Leach and Adam Block, Mt. Lemmon, Arizona.
8. Garner, Rob (2017-10-06). "[Messier 13 \(The Hercules Cluster\)](#)". NASA. Retrieved 2018-04-23.
9. Nemiroff, R. and Bonnell, J. (2019) *APOD: 2019 June 13 - the colors and magnitudes of M13*, NASA. Available at: <https://apod.nasa.gov/apod/ap190613.html> (Accessed: 11 June 2023).

10. *SBIG STL-6303* (no date) *Las Cumbres Observatory*. Available at: <https://lco.global/observatory/instruments/sbig-stl-6303/> (Accessed: 11 June 2023).
11. Burns, M.S. (2022) *A practical guide to observational astronomy*. Boca Raton: CRC Press, Taylor & Francis Group.
12. Narbutis, D., Bridžius, A. and Semionov, D. (2015) 'Structural parameters of star clusters: Signal to Noise Effects', *Open Astronomy*, 24(3). doi:10.1515/astro-2017-0231.
13. Semiconductor Components Industries, LLC (2015) 'KAF-6303 3072 (H) x 2048 (V) Full Frame CCD Image Sensor'. [www.onsemi.com](http://www.onsemi.com).
14. Hainaut, O. (2005) Signal, noise and detection, Signal and Noises. Available at: <http://www.sc.eso.org/~ohainaut/ccd/sn.html> (Accessed: 12 June 2023).
15. Vanderbei, R.J. (no date) *Hertzsprung-Russell diagrams*, *Princeton University*. Available at: <https://vanderbei.princeton.edu/images/NJP/HRdiag.html> (Accessed: 13 June 2023).
16. Vleeming, G. "A photometric study of the open cluster M6 (NGC 6405)." *Astronomy and Astrophysics Supplement Series* 16 (1974): 331-342.